

Neutron stars in the Witten-Sakai-Sugimoto model

Lorenzo Bartolini, Sven Bjarke Gudnason

Institute of Contemporary Mathematics, School of Mathematics and Statistics,
Henan University, Kaifeng, Henan 475004, P. R. China

Abstract

We utilize the top-down holographic QCD model, the Witten-Sakai-Sugimoto model, in a hybrid setting with the SLy4, soft chiral EFT and stiff chiral EFT equations of state to describe neutron stars with high precision. In particular, we employ a calibration that bootstraps the nuclear matter by fitting the Kaluza-Klein scale and the 't Hooft coupling such that the physical saturation density and physical symmetry energy are achieved. We obtain static stable neutron star mass-radius data via the Tolman-Oppenheimer-Volkov equations that yield sufficiently large maximal masses of neutron stars to be compatible with the recently observed PSR-J0952-0607 data as well as all other known radius and tidal deformation constraints.

Contents

1	Introduction	1
2	Witten-Sakai-Sugimoto model	3
3	Holographic nuclear matter: static homogeneous Ansatz	4
4	Isospin asymmetry: time-dependent homogeneous Ansatz	6
5	β-equilibrated matter	8
6	Nuclear matter fit and hybrid equation of state	10
7	Neutron stars	17
8	Conclusion	20

1 Introduction

Neutron matter at densities present in the cores of neutron stars is difficult to study for two reasons: first of all, nucleons at low energy are described dominantly by the strong force, which is hard to tackle due to the nonperturbativity of QCD at strong coupling. The other reason making the study difficult, is that phenomenological models that can capture nuclear physics at low densities are practically impossible to extract reliably to large densities due to the bottom-up approach of such models with a large number of effective couplings that all, in principle, depend on the density. Although perturbative QCD at extremely large densities is able to predict reliably an equation of state [1], such densities are roughly an order of magnitude larger than what is needed for neutron stars.

Holographic QCD models, thanks to their ability to capture a large class of nonperturbative phenomena, have recently been employed with some success to provide predictions for nuclear matter at large densities, and hence represent a valuable tool for the first-principles computation of the equation of state of nuclear matter in regimes typical for the core of neutron stars. Holographic QCD models are a branch of AdS/CFT models developed after Maldacena [2] and Witten's work [3] which are focused on the strong sector, viz. Quantum Chromodynamics and they come generally in two kinds: top-down models derived from string theory constructions, or bottom-up models attempting to mimic the strong gluodynamics of QCD with an appropriate 5-dimensional curved background. In this work, we shall concentrate on the top-down model known as the Witten-Sakai-Sugimoto (WSS) model [3–5], which is especially predictive because it contains only two adjustable parameters, the Kaluza-Klein scale (M_{KK}) and the 't Hooft coupling $\lambda = g^2 N_c$. Usually these parameters are fitted to the meson sector of the theory, reproducing the pion decay constant and the rho-meson mass [4]: when doing so, the model performs rather poorly in

the baryonic sector, while still providing some deep qualitative insights. To overcome this shortcoming, and to try to be as quantitatively precise as the model's approximations allow, in this paper we shall employ a different calibration of the model, which we will justify by the fact that we are working exclusively with baryons in a homogeneous configuration, see below for further discussion on the justification.

Holographic QCD models have been employed earlier in the literature in order to describe neutron stars, in the WSS model with taking the symmetry energy into account [6], in V-QCD [7] which is a highly customized phenomenological version of holographic QCD based on the Veneziano limit – i.e. the limit of a large number of color as well as a large number of quark flavors, in a D3/D7 model [8–10], as well as in a hard-wall model [11] (see Ref. [12, 13] for nice reviews on the topic). Baryons in the WSS model are instantons in the 4-dimensional subspace spanned by the spatial and holographic directions of the 5-dimensional curved AdS-like spacetime and are initially best understood via the BPST flat-instanton approximation [14], which is later shown to be valid only in the large 't Hooft coupling limit [15]. In the context of neutron stars it was shown that the instanton in the pointlike approximation fails to describe tidal deformabilities and baryon masses at the same time [16]. Using instead the homogeneous Ansatz for nuclear matter has previously been quite successful in describing neutron stars, at least barring changing the meson fit of the WSS model to one more appropriate for baryonic matter at finite densities [6]. Although the work [6] holographically takes the symmetry energy [17], charge neutrality and β -equilibrium into account and dynamically determines the crust of the star, their approach has been plagued with unrealistically large symmetry energies, a factor of 30 bigger than its phenomenological value, which in turn shows up as large deviations of physical neutron stars with respect to isospin symmetric neutron stars, for example in the mass-radius data. Such a large overestimation of the symmetry energy can be traced back to the combination of two factors: on one hand one of the gauge fields (the Abelian spatial component) is taken to vanish, an approximation reliable in the large λ limit, but not upon extrapolation to finite λ , while another overall factor of N_c^2 compared to our result arises from a different choice in the definition of the large- N_c isospin number for the nucleon states.

In a recent paper [18], the present authors have employed a conceptually simpler approach to computing the symmetry energy in the WSS model in the approximation of using the homogeneous Ansatz and have shown that it can obtain realistic values, if the model is calibrated with a smaller Kaluza-Klein scale and a larger 't Hooft coupling, than the usual meson fit. Not only is the WSS model able to reproduce the $\sim 32\text{MeV}$ symmetry energy at saturation density, but the slope and second derivatives of the symmetry energy as a function of the density can be made to be consistent with all current experimental constraints – coming both from nuclear physics as well as from neutron star data.

In this paper, we use this result of a realistic symmetry energy as a function of the density and to ensure this is the case, we choose to bootstrap the model by setting the saturation energy to the physically accepted one ($\sim 0.16\text{ fm}^{-3}$), which fixes the Kaluza-Klein scale and then adjust the 't Hooft coupling to obtain the correct value of the symmetry energy at saturation density. It turns out that this calibration scheme gives values of the

couplings very close to those for which the symmetry energy passes all current experimental bounds as a function of the density. As the final ingredient in obtaining realistic neutron stars, requiring a physical equation of state from very low to very high (medium) densities, we take the hybrid approach in this paper as already introduced in Ref. [8], by patching/gluing a very reliable equation of state from nuclear physics at low densities together with our equation of state obtained from the WSS model in our calibration.

This paper is organized as follows. In Sec. 2 we introduce the WSS model as well as our notation. We review the static homogeneous Ansatz in Sec. 3, and include time dependence in Sec. 4. In Sec. 5, we review the relations for obtaining charge neutrality, β -equilibrium and the corresponding thermodynamic relations. We then describe our fit and the hybrid equation of state in Sec. 6 and present the results of the neutron star mass-radius diagrams in Sec. 7. We conclude the paper in Sec. 8 with a discussion and outlook.

2 Witten-Sakai-Sugimoto model

The holographic model we choose to employ for the description of nuclear matter at high density is the Witten-Sakai-Sugimoto model [4, 5], a top-down model of holographic QCD based on the engineering of a couple of stacks of N_f $D8/\overline{D8}$ -branes on the supergravity background sourced by N_c $D4$ -branes. We will work in the configuration of antipodal branes and in the confined geometry phase, so that the flavor branes will extend all the way down to the tip of the cigar subspace, spanning all the holographic direction.

In absence of a mass term for quarks (which we will neglect), the theory after dimensional reduction to five dimensions is given by a Dirac-Born-Infeld action supplemented by a Chern-Simons term. Replacing the Dirac-Born-Infeld action at quadratic order in the field strength, results in a Yang-Mills theory in curved space, with the addition of the topological Chern-Simons term, so that the full action within these approximations read

$$S = -\kappa \text{Tr} \int d^4x dz \left[\frac{1}{2} h(z) \mathcal{F}_{\mu\nu}^2 + k(z) \mathcal{F}_{\mu z}^2 \right] + \frac{N_c}{24\pi^2} \int_{M_5} \omega_5, \quad (1)$$

with the parameter κ and the warp factors $k(z), h(z)$ given by

$$k(z) = 1 + z^2, \quad h(z) = (1 + z^2)^{-\frac{1}{3}}, \quad \kappa = \frac{\lambda N_c}{216\pi^3}, \quad (2)$$

where λ is the 't Hooft coupling and N_c is the number of colors. The $U(2)$ gauge field 1-form \mathcal{A} is split into $SU(2)$ and $U(1)$ factors as

$$\mathcal{A} = A^a \frac{\tau^a}{2} + \widehat{A} \frac{\mathbf{1}_2}{2}, \quad (3)$$

the field strength is given by $\mathcal{F} = d\mathcal{A} + \mathcal{A} \wedge \mathcal{A}$, τ^a are the standard Pauli spin matrices, and the spacetime indices are denoted as

$$\alpha, \beta, \dots = 0, M \quad ; \quad M, N, \dots = i, z \quad ; \quad i, j, \dots = 1, 2, 3. \quad (4)$$

The Chern-Simons 5-form ω_5 is given by

$$\omega_5 = \text{Tr} \left(\mathcal{A} \wedge \mathcal{F}^2 - \frac{i}{2} \mathcal{A}^3 \wedge \mathcal{F} - \frac{1}{10} \mathcal{A}^5 \right), \quad (5)$$

where the powers of forms are understood by the wedge product. The $U(N_f)$ gauge field describes flavor degrees of freedom: In the present work we will assume the presence of two light flavors, thus setting $N_f = 2$ and neglecting contributions from the presence of the strange quark, leaving their inclusion for future improvements. With the notation (3) we can rewrite the Chen-Simons term as

$$S_{\text{CS}} = \frac{N_c}{24\pi^2} \int_{M_5} \text{Tr} \left[3\widehat{A} \wedge F^2 + \widehat{A} \wedge \widehat{F}^2 + d \left(\widehat{A} \wedge \left(2F \wedge A - \frac{i}{2} A^3 \right) \right) \right]. \quad (6)$$

We will assume the gauge fields \widehat{A}_i, A_i to vanish at $z = \pm\infty$, hence we drop the total derivative term. The top-down nature of the model enables it to only rely on two free parameters to be fitted: the 't Hooft coupling λ and the Kaluza-Klein scale M_{KK} . Note that the scale does not appear in any of our expressions when doing calculations within the model: it is the only mass scale of the model, and we can freely choose to work in units of M_{KK} , and then restore the correct power of M_{KK} to obtain the results in physical units.

3 Holographic nuclear matter: static homogeneous Ansatz

In the context of holographic QCD, baryons are described as topological solitons of the flavor fields, and the Witten-Sakai-Sugimoto model is no exception [15]. The Witten-Sakai-Sugimoto soliton can be approximated as a BPST instanton [14, 19] in the limit of large λ : its instanton number is then identified as the baryon number, allowing for the description of nuclei on top of single baryons.

To exactly describe infinite nuclear matter in this model is to solve a many-soliton problem in five-dimensional curved space time: this task is too hard to be carried out for any practical application, so what is done in most cases is to rely on some combination of approximations and educated guesses. A possibility is to arrange individual solitons in a lattice [20], minimizing the free energy density to determine the elementary cell shape and size (hence the density): this kind of approach is generally more reliable at low density, when the individual baryons are well separated, and approximations made to compute the interactions between solitons are well under control.

At densities around nuclear saturation and above, another possible approximation exists: since nucleons are tightly packed, we can approximate their spatial distribution in three-dimensional space to be homogeneous, forming a uniform distribution of continuous nuclear matter. In this process every information about individual baryons is lost, in favor of intensive quantities such as the baryonic and isospin densities. Despite such a configuration not existing under assumptions of homogeneity and regularity of the gauge fields

as shown in Ref. [21], it turns out that it is still possible to define a homogeneous Ansatz by modifying these assumptions, either by enforcing homogeneity at the level of the field strengths [22], or by introducing a discontinuity in the homogeneous gauge fields [23]. For the purpose of this work, we will follow the second route, introducing a discontinuity in the SU(2) gauge field that will source a finite baryon density. The great simplification that this approach produces lies in the reduction of complicated sets of PDEs to more manageable sets of ODEs, the only remaining variable being the holographic coordinate z (and time, whose inclusion we will discuss in the next section). The homogeneous Ansatz in the static approximation is given by the gauge field configuration

$$\mathcal{A}_0^{\text{cl}} = \frac{1}{2}\widehat{a}_0\mathbf{1}, \quad \mathcal{A}_i^{\text{cl}} = -\frac{1}{2}H\tau^i, \quad \mathcal{A}_z^{\text{cl}} = 0, \quad (7)$$

with $\widehat{a}_0 = \widehat{a}_0(z)$, $H = H(z)$ being functions of only the holographic coordinate z .

The function $H(z)$ encodes baryonic density, as it can be thought of as the space-averaged many-soliton distribution. It does so in a nontrivial way if we allow it to be discontinuous: for simplicity we will assume a discontinuity is present in the function $H(z)$ at $z = 0$, which is the coordinate at which single solitons sit to minimize energy, however it is possible to consider configurations with more discontinuities located at finite $z = \pm z_0$ (see Ref. [24] for the treatment in both the Witten-Sakai-Sugimoto and the VQCD models). The baryon density d is given as

$$\begin{aligned} d &= \frac{1}{32\pi^2} \int_{-\infty}^{+\infty} dz \epsilon^{MNPQ} \text{Tr} F_{MN} F_{PQ} \\ &= -\frac{3}{8\pi^2} \int_{-\infty}^{+\infty} dz H' H^2 \\ &= -\frac{1}{8\pi^2} [H^3]_{z=0^+}^{z=+\infty} - \frac{1}{8\pi^2} [H^3]_{z=-\infty}^{z=0^-}. \end{aligned} \quad (8)$$

We see immediately that a continuous function $H(z)$ would not be able to describe nuclear matter at any finite density: it has to be an odd, discontinuous function of z . We choose the function $H(z)$ to be vanishing at the UV boundary $z = \pm\infty$, so that we are left with an IR boundary condition for $H(z)$ reading

$$H(0^\pm) = \pm (4\pi^2 d)^{\frac{1}{3}}. \quad (9)$$

From now on, we will always perform integrals over z on the "positive z " half of the connected branes, accounting for the symmetry of the integrands with an overall factor of two. Note that despite the discontinuity in $H(z)$, the field strengths F_{MN}^a are still continuous, even functions of z (though in general not differentiable at $z = 0$).

The asymptotic UV value assumed by the function $\widehat{a}_0(z)$ is mapped into the baryonic chemical potential as per the standard holographic dictionary: we can then impose boundary conditions

$$\widehat{a}'_0(0) = 0, \quad \widehat{a}_0(\infty) = \mu, \quad (10)$$

$$H(0) = (4\pi^2 d)^{\frac{1}{3}}, \quad H(\infty) = 0, \quad (11)$$

and numerically solve the equations of motion

$$hH^3 - \frac{1}{2}\partial_z(kH') - \frac{N_c}{32\pi^2\kappa}H^2\hat{a}'_0 = 0, \quad (12)$$

$$\partial_z(k\hat{a}'_0) + \frac{3N_c}{16\pi^2}H^2H' = 0. \quad (13)$$

With the normalization chosen for the asymptotics of \hat{a}_0 , the baryon number chemical potential μ_B is given by

$$\mu_B = \frac{N_c}{2}\mu. \quad (14)$$

For every value of the parameter μ , the corresponding thermodynamic equilibrium value of the density $d(\mu)$ is given by minimizing the free energy Ω , holographically dual to the on-shell action as $\Omega = -S^{\text{on-shell}}$. The baryonic phase is favored over the vacuum when $\Omega(d, \mu) \leq 0$, a condition that is satisfied for $d(\mu) \geq d_0(\mu_{\text{onset}})$. The value d_0 is the model prediction for nuclear saturation density of symmetric matter, and will play an important role in our choice for the fit of the free parameters λ, M_{KK} .

4 Isospin asymmetry: time-dependent homogeneous Ansatz

The time-independent configuration introduced in the previous section only accounts for symmetric baryonic matter. This can be understood by thinking about the single-baryon: a single static soliton is a classical object, that carries no information about the nucleon states. To have a spectrum including isospin states we have to perform moduli space quantization [14]: an arbitrary rotation in $SU(2)$ -space that corresponds to a zero mode is introduced by performing the transformation $\tau^i \rightarrow a\tau^i a^{-1}$. The orientation matrix a is then promoted to a time-dependent operator $a(t)$, in terms of which it is possible to compute an effective quantum mechanical Hamiltonian that will give the single-baryon spectrum. The same procedure can be applied to the homogeneous Ansatz, as described in detail in Ref. [18]. In particular, the homogeneous Ansatz is similar in its structure to the BPST instanton, but simpler in that it lacks the position and size moduli. We then follow the same procedure in the treatment of rotational moduli $a(t) \in SU(2)$, and we define the angular velocity χ^i as:

$$\chi^i \equiv -i \text{Tr} (a^{-1} \dot{a} \tau^i). \quad (15)$$

The introduction of the $SU(2)$ moduli and their time dependence turns on new components of the gauge field, so that the new homogeneous Ansatz for the iso-rotating configuration is given by

$$\mathcal{A}_0 = Ga\chi \cdot \tau a + \frac{1}{2}\hat{a}_0, \quad \mathcal{A}_i = -\frac{1}{2}(Ha\tau^i a + L\chi^i), \quad \mathcal{A}_z = 0, \quad (16)$$

The classical action obtained from the time-dependent homogeneous Ansatz following the prescription introduced in Ref. [25] to choose the correct Chern-Simons term, is

$$\begin{aligned}
S_{\text{YM}} &= -\kappa \int d^4x \int_0^\infty dz \left[-8hH^2 \left(G + \frac{1}{2} \right)^2 \boldsymbol{\chi} \cdot \boldsymbol{\chi} + 3hH^4 \right. \\
&\quad \left. + k \left[(L')^2 - 4(G')^2 + 8(KH)^2 \right] \boldsymbol{\chi} \cdot \boldsymbol{\chi} + 3k(H')^2 - k(\hat{a}'_0)^2 \right], \\
S_{\text{CS}} &= -\frac{3N_c}{8\pi^2} \int d^4x \int_0^\infty dz \hat{a}_0 H' H^2 \\
&\quad + \frac{N_c}{4\pi^2} \int d^4x \int_0^\infty dz \left(2LH' \left(G + \frac{1}{2} \right) + LHG' \right) H \boldsymbol{\chi} \cdot \boldsymbol{\chi}, \quad (17)
\end{aligned}$$

from which the equations of motion for the fields $H(z), \hat{a}_0(z), L(z), G(z)$ can be derived:

$$hH^3 - \frac{1}{2} \partial_z(kH') - \frac{N_c}{32\pi^2\kappa} H^2 \hat{a}'_0 = 0, \quad (18)$$

$$\partial_z(k\hat{a}'_0) + \frac{3N_c}{16\pi^2} H^2 H' = 0, \quad (19)$$

$$\partial_z(kG') - 2hH^2 \left(G + \frac{1}{2} \right) + \frac{N_c}{32\pi^2\kappa} H^2 L' = 0, \quad (20)$$

$$\partial_z(kL') + \frac{N_c}{8\pi^2\kappa} H [HG' + (1 + 2G)H'] = 0. \quad (21)$$

The equations of motion have to be supplemented with adequate boundary conditions: following Ref. [25] we choose them so to cancel the infrared localized terms in the variation of the action, which amounts to require:

$$\left[G'(0) + \frac{N_c}{32\pi^2\kappa} H(0)^2 L(0) \right] = 0, \quad (22)$$

$$L'(0) = 0. \quad (23)$$

The field A_0 encodes via the holographic dictionary the information on the isospin density n_I and chemical potential μ_I . This can be understood as follows: $G(z)$ can be thought of as a holographic profile for the angular velocity χ^i , which can be traded for the corresponding angular momentum and then canonically quantized in the moduli space approximation. The resulting operator is identified with both spin and isospin operators (an artifact of the spherical symmetry of the setup). When we do this, the resulting quantum Hamiltonian operator is given by

$$H = \frac{I^2}{2V\Lambda} + VU, \quad (24)$$

with V being the three-dimensional (infinite) volume, I^2 is the squared isospin operator, and Λ and U given by

$$\begin{aligned}\Lambda &= 2\kappa \int_0^\infty [2hH^2(2G+1)^2 + k((L')^2 + 4(G')^2)] dz, \\ U &= \kappa \int_0^\infty [3hH^4 + 3k(H')^2 + k(\hat{a}'_0)^2] dz.\end{aligned}\tag{25}$$

They are respectively the moment of inertia of a rigid rotor and its internal energy density, which in our physical setup corresponds to the energy density of symmetric nuclear matter.

From this Hamiltonian operator, we obtain the energy per nucleon of an isospin state $|i, i_3\rangle$, from which we can read off the symmetry-energy parameter of infinite nuclear matter $S_N(d)$:

$$\frac{E}{A} = \frac{U}{d} + S_N(d)\beta^2 + \mathcal{O}(V^{-1}), \quad S_N(d) = \frac{d}{8\Lambda},\tag{26}$$

with $\beta = (N - Z)/A$ being the isospin asymmetry parameter.

We will also need the energy density since our final aim is to obtain an equation of state for isospin asymmetric nuclear matter in β -equilibrium with leptons. From the expressions above, the energy density of isospin-asymmetric matter is obtained from U, Λ as

$$\mathcal{E} = \frac{E}{V} = \frac{i_3^2}{2V^2\Lambda} + U = \frac{1}{2\Lambda}n_I^2 + U.\tag{27}$$

The isospin chemical potential μ_I can be obtained from the expression above by differentiating with respect to n_I , so that

$$\mu_I = \frac{\partial \mathcal{E}}{\partial n_I} = \frac{n_I}{\Lambda}.\tag{28}$$

Note that we have defined n_I from the isospin quantum number i_3 , which assume values $\pm 1/2$ for the ground states. We choose to identify the positive eigenvalue to correspond to the proton, and the negative one to the neutron, following conventions from nuclear physics. With this choices, if the nuclear matter is rich in neutrons (as we expect it to be following beta equilibrium and charge neutrality), we will have $n_I < 0$ and correspondingly also the isospin chemical potential μ_I will be negative due to Eq. (28).

5 β -equilibrated matter

The presence of the symmetry energy favors isospin-symmetric matter: the neutron rich matter that composes the core neutron stars is the result of the presence of negatively charged leptons that impose electric charge neutrality to the system. The leptons with their (anti)neutrinos, the neutrons and the protons are in equilibrium with respect to β -decay. This condition, together with charge neutrality, is sufficient to calculate the

fractions of each particle species at any given density. As discussed in Ref. [18] with the same normalizations used in this work, the imposition of β -equilibrium (together with the decoupling of the neutrinos) and electric charge neutrality lead respectively to the conditions

$$\mu_\ell = \mu_N - \mu_P = -\mu_I, \quad \ell = e, \mu, \quad (29)$$

$$\frac{1}{2}d + n_I = \sum_\ell n_\ell, \quad (30)$$

where μ_X is the chemical potential of the particle species X and we accounted for the presence of electrons (e) and muons (μ) in equilibrium with protons (P) and neutrons (N), while neglecting the presence of the heavier taus (τ).

The leptonic number densities n_ℓ are taken as originating from the free energy of a (massive) Fermi gas:

$$\Omega_\ell = -\frac{1}{24\pi^2} \Theta(\mu_\ell - m_\ell) \left[(2\mu_\ell^2 - 5m_\ell^2) \mu_\ell \sqrt{\mu_\ell^2 - m_\ell^2} + 3m_\ell^4 \log \left(\frac{\sqrt{\mu_\ell^4 - m_\ell^4} + \mu_\ell}{m_\ell} \right) \right], \quad (31)$$

from which follows

$$n_\ell(\mu_\ell) = \Theta_H(\mu_\ell - m_\ell) \frac{(\mu_\ell^2 - m_\ell^2)^{\frac{3}{2}}}{3\pi^2}. \quad (32)$$

We will approximate the electrons to be massless, while keeping the muons massive with $m_\mu^{\text{phys}} = 105.66 \text{ MeV}$, while the parameter appearing in the equations is the corresponding value in units of M_{KK} , $m_\mu = m_\mu^{\text{phys}} M_{\text{KK}}^{-1}$.¹

Inserting Eq. (32) into the charge-neutrality condition (30) and using the β -equilibrium condition (29), we obtain an implicit solution for the isospin density, n_I , as a function of the baryon density d (note that with the present conventions, n_I is always negative in neutron rich matter, and that Λ is always positive by construction, as appropriate for its interpretation as a moment of inertia):

$$\frac{n_I^3}{3\pi^2 \Lambda^3} \left[\Theta_H(-n_I) + (1 - R^{-2} m_\mu^2)^{\frac{3}{2}} \Theta_H(-R - m_\mu) \right] + n_I + \frac{1}{2}d = 0, \quad R \equiv n_I/\Lambda. \quad (33)$$

From $n_I(d)$ it is then possible to compute the density of every particle species as

$$n_P(d) = \frac{1}{2}d + n_I(d), \quad (34)$$

$$n_N(d) = \frac{1}{2}d - n_I(d), \quad (35)$$

$$n_e(d) = \frac{1}{3\pi^2} (\mu_I(d)^2)^{\frac{3}{2}}, \quad (36)$$

$$n_\mu(d) = \frac{1}{3\pi^2} (\mu_I(d)^2 - m_\mu^2)^{\frac{3}{2}}. \quad (37)$$

¹Note that by doing this we are introducing another energy scale in the model: since the value of m_μ depends on the choice of the value M_{KK} , such parameter can no longer be factorized out from the equations.

To build an equation of state for the matter we just described, we need now to compute the total energy density and pressure. The building blocks are the energy densities U and pressure P_0 of symmetric nuclear matter, the contributions \mathcal{E}_I and P_I due to isospin asymmetry, and the contributions \mathcal{E}_ℓ, P_ℓ of leptons.

We already know an expression for U from Eq. (25), which we can use to compute the pressure P_0 using μ_B and d

$$P_0 = -U + \mu_B d. \quad (38)$$

For the contributions arising from isospin asymmetry, we make use of the known relations (28), (27):

$$\mathcal{E}_I = \frac{1}{2\Lambda} n_I^2, \quad (39)$$

$$P_I = -\mathcal{E}_I + \mu_I n_I = \frac{1}{2\Lambda} n_I^2 = \mathcal{E}_I. \quad (40)$$

Finally, for the leptons we can use the fact that in a homogeneous system $P = -\Omega$ holds, so that we can compute P_ℓ directly from Eq. (31), from which the energy density follows

$$\begin{aligned} \mathcal{E}_e + \mathcal{E}_\mu &= \Omega_e + \Omega_\mu + \mu_e n_e + \mu_\mu n_\mu \\ &= \Omega_e + \Omega_\mu - \mu_I n_P \\ &= \Omega_e + \Omega_\mu - \frac{n_I}{\Lambda} \left(\frac{1}{2} d + n_I \right), \end{aligned} \quad (41)$$

where we have made use of charge neutrality and β -equilibrium. As a result, we can finally write the total energy density and pressure as

$$\mathcal{E} = U + \mathcal{E}_I + \mathcal{E}_e + \mathcal{E}_\mu, \quad (42)$$

$$P = P_0 + P_I - \Omega_e - \Omega_\mu, \quad (43)$$

with every quantity involved being a function of only the baryon density d .

6 Nuclear matter fit and hybrid equation of state

It is well known that the most common fit of the Witten-Sakai-Sugimoto model ($M_{\text{KK}} = 949\text{MeV}$, $\lambda = 16.6$) performs very well in the mesonic sector, but that its quantitative reliability when employed to compute quantities of the baryonic sector is somewhat lacking (in particular the masses of the baryons are largely overestimated, together with the binding energies of nuclei). When we move to the dense nuclear matter described by the homogeneous Ansatz, the situation gets worse and contact with phenomenology is lost. For example, the saturation density for $\lambda = 16.6$ is found to be $d_0^{\lambda=16.6} = 0.00385 M_{\text{KK}}^3$, while the symmetry energy at saturation is of order $S_N^{\lambda=16.6}(d_0^{\lambda=16.6}) \simeq 0.1 M_{\text{KK}}$: when the value $M_{\text{KK}} = 949\text{MeV}$ is plugged into these expressions, the results are respectively

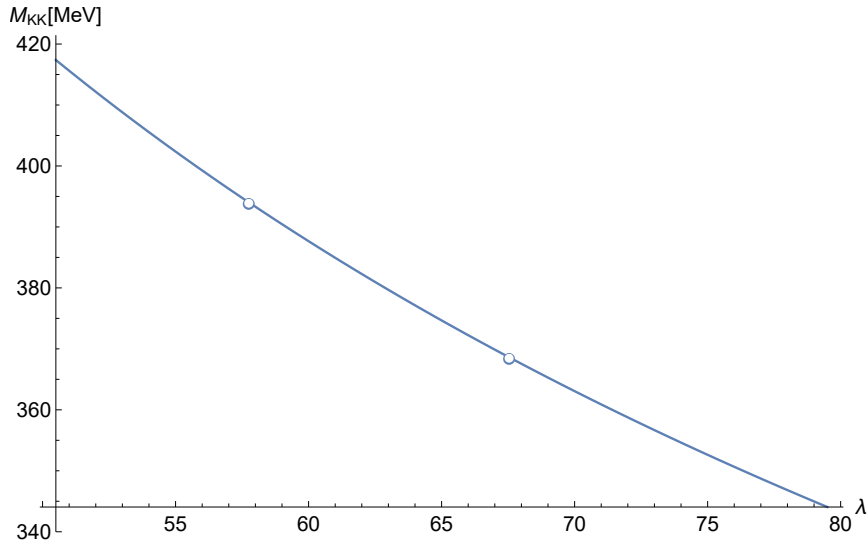


Figure 1: The curve $M_{KK}(\lambda)$ that fits the saturation density of symmetric nuclear matter to its phenomenological value of $d_0^{\text{phys}} = 0.16 \text{ fm}^{-3}$. The two dots marked on the plot correspond to the two fits we employed, corresponding to the upper and lower bounds on the symmetry energy of 32.8 MeV and 30.6 MeV, respectively.

$d_0 = 0.43 \text{ fm}^{-3}$ and $S_N(d_0) = 97 \text{ MeV}$. If we ignore these issues and try to build the core of neutron stars with this fit, we unsurprisingly find that they never reach $1.5M_\odot$, and their radius can at most be slightly larger than 7km. Realistic values for the highest mass for a stable star and for the average radii have been obtained with a fully holographic equation of state (though with the phenomenological input of the surface tension of the domain wall between nuclear matter and vacuum) from the Witten-Sakai-Sugimoto model in Ref. [6]: to obtain a realistic-looking neutron star while keeping $M_{KK} = 949 \text{ MeV}$, it is necessary to decrease λ to around the value $\lambda = 10$, with the results being highly sensitive to changes around this value. Realistic masses and radii for neutron stars as functions of the model parameters λ, M_{KK} within this setup have been further explored in Ref. [26]. However, even producing stars with adequate radii and masses, nuclear matter inside the stars of Ref. [6] fails to be as rich in neutrons as we expect in neutron stars: this is due to the extremely high value of the symmetry energy, which pushes matter towards isospin symmetric configurations, and remains true even if we adopt the lower values of symmetry energies found in Ref. [18], as long as we adopt fits defined in the ‘‘QCD window’’ introduced in Ref. [26]. Our aim is to describe realistic neutron star cores and connect the equation of state from holography with a phenomenologically accurate equation of state at lower energy densities: within this approach, it makes little sense to employ a fit that overestimates physical quantities that are crucial in the formation of the structure of neutron stars by a factor of roughly three. Moreover, the fit is done on single-particle properties, but information on individual particles is lost when employing the homogeneous Ansatz, which does not connect smoothly to the finite particle number setup.

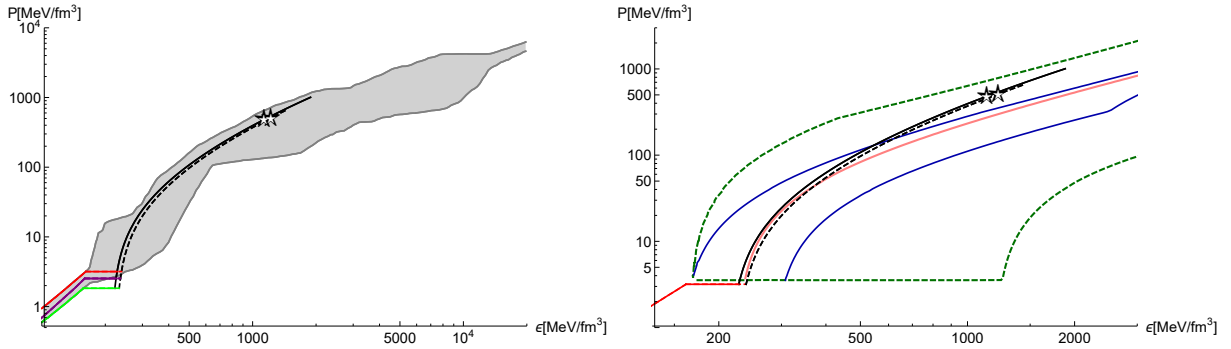


Figure 2: Left panel: in red (green) the low-density equation of state obtained from the upper (lower) bound derived from CEFT, in purple the low-density SLy4 equation of state, in black the branches of the equations of state computed from the WSS model, the gray-shaded area marks currently accepted bounds for the EOS of nuclear matter constrained by neutron stars data. The solid (dashed) line represents the fit that achieves $S_N = 32.8$ MeV ($S_N = 30.6$ MeV) at saturation density $d_0 = 0.16 \text{ fm}^{-3}$. The star markers in the plot represent the pressure and density of the heaviest stable static neutron stars allowed by that particular equation of state (the left-most star marker corresponds to the solid line). Right panel: the hybrid stiff-WSS EOS compared with model independent bounds from Ref. [27], derived from pQCD and shown with a dashed green line. EOS lying within the dark blue lines have an upper-bound on the speed of sound at the conformal value $c_s^2 < 1/3$. The pink line represents the limiting case in which the speed of sound is constant along the EOS.

We hence propose another choice of fit for the free parameters of the Witten-Sakai-Sugimoto model, expected to give precise results when applied to highly dense matter, especially in the context of the homogeneous Ansatz. The first quantity we fit is the nuclear saturation density for symmetric matter: phenomenologically this value lies at about 0.16 fm^{-3} . The value of the model-derived saturation density in units of M_{KK} does not depend on M_{KK} itself, so we only need to compute the value $d_0(\lambda)$ for a wide range of values of λ , then impose the condition

$$d_0(\lambda)M_{\text{KK}}^3 = 0.16 \text{ fm}^{-3}. \quad (44)$$

This defines the function $M_{\text{KK}}(\lambda)$ we plot in figure 1. The second choice we employ to eliminate any further freedom is to have a realistic symmetry energy at saturation density. The phenomenologically accepted values range between 30.6 MeV and 32.8 MeV: we fit the model to both values, so to produce an "error bar" for our predictions. As a result, the two fits for which we will present results correspond to

$$\lambda = 67.55 \quad , \quad M_{\text{KK}} = 368.6 \text{ MeV} \quad \Rightarrow \quad S_N(d_0) = 30.6 \text{ MeV}, \quad (45)$$

$$\lambda = 57.76 \quad , \quad M_{\text{KK}} = 394.01 \text{ MeV} \quad \Rightarrow \quad S_N(d_0) = 32.8 \text{ MeV}. \quad (46)$$

Using these fits we build the equation of state for holographic matter, which we assume to be the appropriate description at densities above saturation: to describe lower-density regions of the neutron star, namely the crust, we would need a more refined construction, possibly deviating from the homogeneous approximation, for example nuclear pasta phases. A similar construction was performed in Ref. [6], where a crust was built from the mixed phase of lumps of nuclear matter in β -equilibrium, immersed in a gas of leptons, with the surface tension of the domain wall, separating the phases, as the parameter to regulate the onset of the transition from homogeneous matter to the mixed phase. Here we follow another possible approach, that of a "hybrid" equation of state: within this framework, we forego the attempt of building the full equation of state from a single model, and instead patch together equations of state coming from different models, each derived within the domain of applicability of the models themselves. In particular, equations of state for low-density nuclear matter are already developed with a higher precision than the one we can hope to achieve within the holographic model: we then choose to employ a set of three different low energy equations of state: a soft and a stiff one, taken as the two limiting scenarios from chiral EFT interactions as described in Ref. [28], and the SLy4 equation of state tabulated in Ref. [29, 30], which we then match at larger densities with the holographic equation of state described in the previous section: the criteria we require for the matching are that the pressure and baryon number density are continuous at the junction.

The density at which the patching is performed is weakly dependent on the fit choice and on the low-density equation of state employed, in the range of $d_P \in (1.032d_0, 1.059d_0)$, with lower values for the soft equation of state, intermediate values around $1.045d_0$ for the SLy4, and the upper bound for the stiff equation of state.

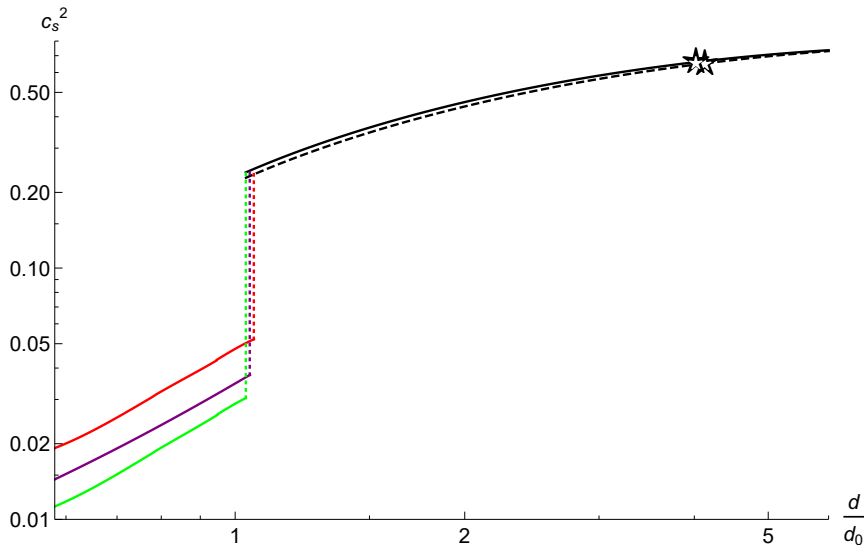


Figure 3: The speed of sound for the three hybrid equations of state presented in Fig. 2 as function of density in units of the saturation density d_0 . The star markers represent the speed of sound reached inside the heaviest stable static neutron stars allowed by the corresponding equation of state.

By doing this, we obtain the equations of state shown in Fig. 2, where they are compared with currently established bounds.

From the equations of state, we can numerically compute the speed of sound: the resulting plot is shown in Fig. 3, and it shows the presence of a discontinuity at the density corresponding to the junction between the two equations of state from different models. The holographic equation of state is highly stiff as it rapidly crosses the conformal value of $c_s^2 = 1/3$: this is a feature it shares with many equations of state derived from holography, but even for this category it achieves very high sound speeds, with the highest speed present in stable neutron stars ranging in the interval $c_s^2 \in (0.652, 0.660)$, depending on the choice of fit (the two star markers in Fig. 3 pinpoint these values). Note also that the stability of the stars is what limits the speed of sound to these values: the equation of state extrapolated to higher densities produces higher velocities, which however are never reached in stable stars.

We can also test our choices of fit against the particle populations: using Eqs. (34) to (37) we can compute the number densities of each species of particles, and compare them with those of the SLy4 equation of state at the junction point. The results are presented in the two panels of Fig. 4: we can see from the right panel that, while at the junction point the SLy4 populations do not fall precisely within the predictions of our two fit choices, the mismatch is quite small, and the results from the holographic model are well in the correct ballpark. From this result alone it would seem that a favored fit would lie closer to that of Eq. (46) corresponding to $S_N(d_0) = 32.8$ MeV, a tendency that will be reinforced in the next section by comparing the results for the tidal deformabilities of neutron stars.

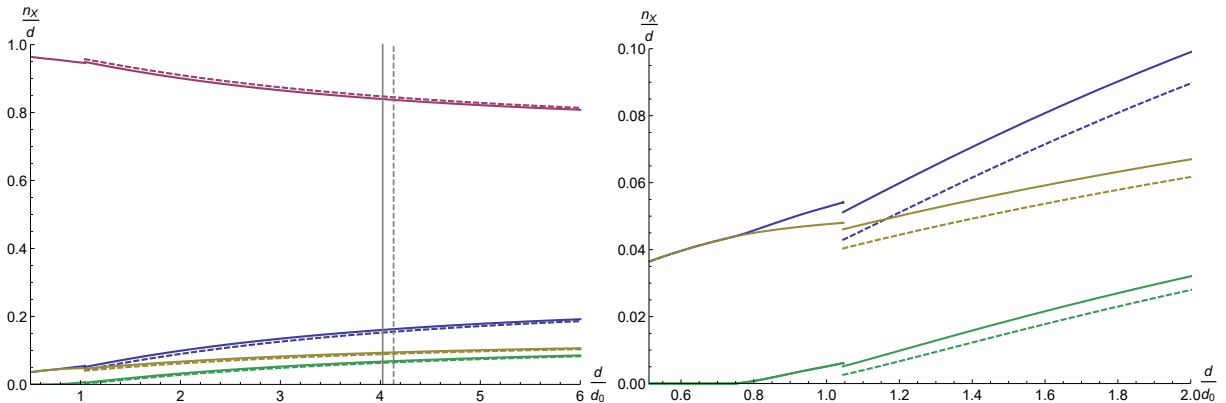


Figure 4: Particle fractions as function of the density (in units of the saturation density), with the curves from top to bottom corresponding to neutrons (dark red), protons (purple), electrons (yellow) and muons (green). The solid and dashed lines are for the two different fits, see the caption of Fig. 2. The left panel covers the entire range relevant for even our heaviest neutron stars, whereas the right panel zooms in around the densities where we have patched the SLy4 and the WSS equation of state together.

Before applying the computed equations of state to neutron stars, let us comment on the shortcomings of the approach and approximations we employed. The first noticeable feature shared by the equations of state plotted in Fig. 2 is the discontinuity in the energy density \mathcal{E} , represented by the horizontal segment that connects the low-density branches to the holographic part: we regard this unexpected phase transition as an artifact due to the failure of the model, the Ansatz and the fit choice, to reproduce the correct onset value of the baryonic chemical potential, giving the value of 1345.5 MeV (1409.9 MeV) for $\lambda = 57.76$ ($\lambda = 67.55$). A more sophisticated construction of the transition between the two equations of states could in principle ameliorate the problem: at lower densities, just around saturation, we expect the homogeneous approximation to lose reliability, while configurations where baryons can individually be resolved become more realistic (e.g. lattice configurations). Connected to this issue, is the sharp discontinuity in the speed of sound, as manifest in Fig. 3. In the same spirit, we should not regard the transition between the two equations of state as being exhaustively described by our construction since at the patching density d_P the properties of nuclear matter abruptly change behavior to that of the high-density regime: again, we can expect that introducing at least one intermediate description could provide a more realistic speed of sound around these densities. As an example, in Ref. [31] nuclear matter built from an instanton Ansatz leads to a speed of sound at saturation density of roughly $c_s^2(d_0) \simeq 0.025$, a value close to the ones reached by the three phenomenological equations of state we employed at low density: this can be indicative that the instantonic description does indeed capture more reliably the physics of nuclear matter in this regime, though we have to keep in mind that the brane configuration in Ref. [31] is different from the one we have employed. The idea that the homogeneous approximation is to be held responsible for this sharp jump in the speed of sound is

also strengthened by the observation that a similar behavior is shared between different constructions that employ the same description: in particular, it is present in Ref. [6], which still uses the WSS model, but contains a holographic EOS also for the crust of the star, and it is present in VQCD as can be noted in the review [12].

Lastly, we should comment on the high-density regime: we argued that the homogeneous Ansatz becomes increasingly reliable as the density increases. While this is intuitively true, it still does not take into account other possible effects that can lead to different physics. In particular, we need to address two shortcomings of our approach that manifest themselves in the high-density limit.

The first one is that in the present work we have not included the possibility of a phase transition to quark matter: as pointed out in Ref. [32], it is expected that matter in the heaviest neutron stars exhibits a deconfined phase, and this behavior is reflected in the speed of sound approaching values close to the conformal limit $c_s^2 = 1/3$ already around the TOV densities. Our choice of not exploring the possibility of this phase is mostly due to practical reasons: in the WSS model with antipodal flavor branes, the inclusion of quark matter is only possible in the deconfined geometry (i.e. the black brane horizon sources the quark baryonic charge), which requires (in the absence of backreaction of the flavor branes on the geometry) high temperatures. In principle, including backreaction could lead to such a phase even in the low-temperature regime, since a high baryon density can also induce the formation of a horizon in the bulk, which in turn would source a non-topological baryon number, to be identified as generated by individual quarks. However, the full backreaction of Witten’s background is extremely challenging, and its development is far from achieved (though the first order in $\frac{N_f}{N_c}$ has been developed, at least in the “smeared” configuration of the flavor branes, see Ref. [33]). Another possibility would be to abandon the antipodal branes configuration, and then adopt the decompactified limit as in Ref. [31, 34, 35]: in this way, at the price of changing the branes’ UV boundary condition (hence the dual UV theory) and introducing the dynamics of the embedding of the flavor branes to the equations of motion, it is possible to describe quark matter in the low-temperature regime [34], and possibly even quarkyonic matter [35]. We are leaving the investigation of these possibilities to future developments.

The second limitation we need to point out is that, even if we include the high-density regime, we cannot expect it to converge to the correct asymptotic behavior of perturbative QCD: this is a fundamental shortcoming of the model, that fails at reproducing asymptotic freedom. As a result, even including a phase transition at high density, there is little hope that the equation of state from Fig. 2 connects with the pQCD limit. Despite this limitation, we stress that the part we computed of the equation of state, does not violate the constraints set by Ref. [27], as shown in the right panel of Fig. 2. To establish the comparison, we plot the same bounds as in Ref. [27], together with our hybrid stiff-WSS EOS, as appropriate for the bounds (chosen in the latter reference), obtained by matching the high-energy pQCD EOS with the low-energy CEFT stiff EOS at $d = 1.1d_0$. Our EOS is found to only lay below the lower bound in a very small range of values around the hybridization density: this however is simply due to the choice performed in Ref. [27] to take the low-density limit to be identified with $d = 1.1d_0$, and interpolate between that

particular value and the high-density one from pQCD, while for us the critical density of hybridization is around $d_P^{\text{stiff}} = 1.06d_0$. Choosing our d_P^{stiff} as a low density limit would result in new bounds which establish the hybrid EOS to be consistent with pQCD bounds at least up to TOV densities. However, as already pointed out, we expect the WSS model to exhibit corrections to the computed behavior around saturation density, so we leave a complete analysis around these regions to future works, when a more quantitatively trustable approach will be available.

7 Neutron stars

We finally want to derive properties of neutron stars built with the equation of state we just constructed: to do so, we solve numerically the Tolman-Oppenheimer-Volkov (TOV) equations for a range of central pressures (P_0). Each solution will provide a neutron star with central density P_0 , radius $R(P_0)$, mass $M(P_0)$ and tidal deformability $\Lambda(P_0)$. The TOV equations are given by

$$\frac{dP}{dr} = -G(\mathcal{E} + P) \frac{m + 4\pi r^3 P}{r(r - 2Gm)}, \quad (47)$$

$$\frac{dm}{dr} = 4\pi r^2 \mathcal{E}, \quad (48)$$

and describe static neutron stars, hence we are neglecting the effects of rotation in this analysis. We supplement the equations with the third one

$$\begin{aligned} r \frac{dy}{dr} = & -y^2 - \frac{4\pi G r^2 \left(5\mathcal{E} + 9P + \frac{\mathcal{E}+P}{c_s^2} \right) - 6}{1 - \frac{2GM}{r}} - \frac{y [1 - 4\pi G r^2 (\mathcal{E} - P)]}{1 - \frac{2GM}{r}} \\ & + \frac{4G^2 (M + 4\pi P r^3)^2}{r^2 \left(1 - \frac{2GM}{r} \right)^2}. \end{aligned} \quad (49)$$

From the solution of Eqs. (47)-(48) we produce relations between mass and radius, and employing Eq. (49) with the boundary condition $y(0) = 2$, we obtain the relation between mass and tidal deformability Λ , with the definition

$$\Lambda = \frac{2k_2}{3c^2}. \quad (50)$$

In the above equation, $c = \frac{GM}{R}$ is the compactness of the star, while k_2 is the tidal Love number, defined by:

$$\begin{aligned} k_2 = & \frac{8c^5}{5} (1 - 2c)^2 [2 - y_R + 2c(y_R - 1)] \times \{2c [6 - 3y_R + 3c(5y_R - 8)] + \\ & + 4c^3 [13 - 11y_R + c(3y_R - 2) + 2c^2(1 + y_R)] \\ & + 3(1 - 2c)^2 [2 - y_R + 2c(y_R - 1)] \ln(1 - 2c)\}^{-1}. \end{aligned} \quad (51)$$

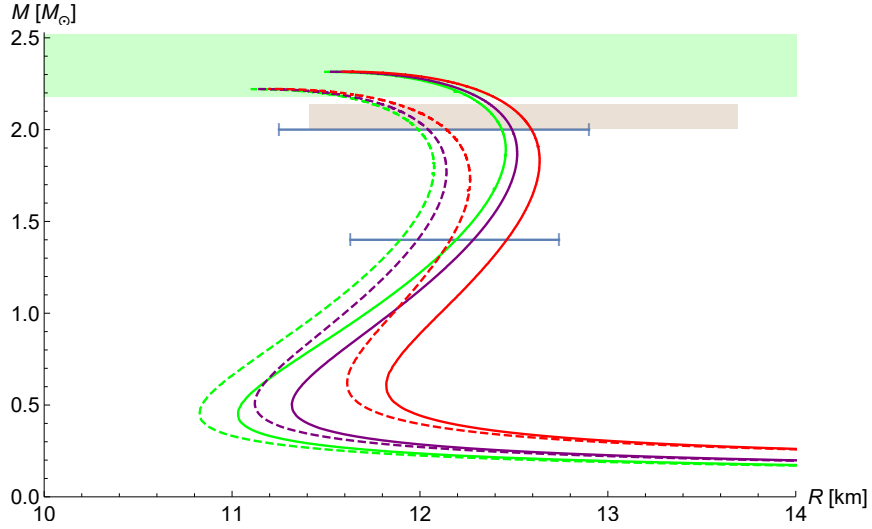


Figure 5: The mass-radius diagram of neutron stars in our model. In red (green), the curves corresponding to neutron stars built from the WSS equation of state hybridized with the stiff (soft) CEFT one. In purple, the curves corresponding to neutron stars built from the WSS equation of state hybridized with SLy4. For every color, the solid (dashed) line represent the fit that achieves $S_N = 32.8 \text{ MeV}$ ($S_N = 30.6 \text{ MeV}$) at saturation density $d_0 = 0.16 \text{ fm}^{-3}$. The blue horizontal error bars are calculated from ^{208}Pb neutron skin thickness [36], while the gray-shaded region is from Ref. [37]. The light green shaded area represents the measured mass of PSR J0952-0607 and represents a lower bound for the maximal achievable mass by a stable (static) neutron star.

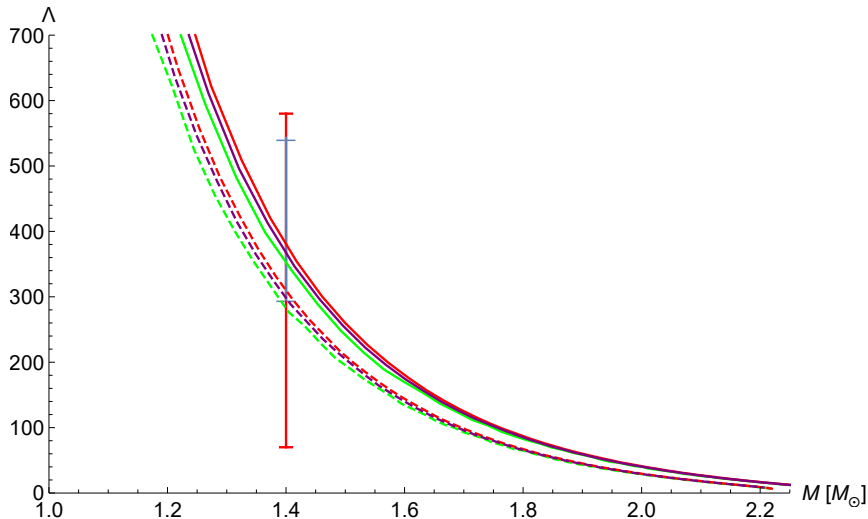


Figure 6: Tidal deformability for the hybrid neutron stars of Fig. 5 for the two different fits. The color coding follows the same conventions as in Fig. 5. The blue bound is from Ref. [36], whereas the red bound is from Ref. [38].

In particular the mass-radius curve represents the best test currently available for neutron stars models: our results for this relation are provided in Fig. 5, where we plot in purple the data for the stars generated by the SLy4-WSS equation of state, and in red (green) the data for the ones generated by the stiff (soft) CEFT-WSS equation. Remarkably, all the hybrid equations of state, derived from fitting the WSS model to saturation density and symmetry energy, result in neutron stars satisfying every constraint in the mass-radius curve, and achieve rather high maximum masses for stable stars, compatible with the highest mass measured to date, i.e. $2.35 \pm 0.17 M_{\odot}$ of PSR J0952-0607².

In Fig. 6 we plot the tidal deformability against the mass of the star: the tidal deformability $\Lambda_{1.4}$ for a neutron star of mass $1.4 M_{\odot}$ ends up being in good agreement with currently established bounds in the case of the fit corresponding to $S_N(d_0) = 32.8$ MeV for all three low-density EOSs, while the other fit choice is either at tension with or slightly outside the bound from one of the references adopted (despite both choices being in good agreement with the more loose bound from Ref. [38]); another hint (together with the proton fraction at the junction density) that possibly the favored fit is one closer to Eq. (46).

The SLy4-WSS equation of state can be seen as one of intermediate stiffness, between the soft and stiff CEFT ones: in particular, since we used the extremal upper and lower bounds dictated by CEFT, and since the junction density is determined to be lower than the value of $1.1d_0$ employed in Ref. [28] as the density at which the equation of state changes to a polytropic piecewise expansion, we conclude that these two curves also represent boundaries of a region in the M - R plane that encompass all possible hybridization of any choice of low-density equation of state, hybridized with our particular WSS one. Thus,

²Though this constraint does not necessarily need to be satisfied by static objects since PSR J0952-0607 is a pulsar with a 1.41ms rotation period.

we conclude that the consistency of the M - R curves with current observations is a robust feature of our holographic hybrid equation of state: of course the situation can change once we adopt refinements to the hybridization process (such as ones mentioned in the previous section), so we restrict ourselves to only remark that, in the presence of these quite crude approximations, the WSS model can provide an EOS for densities above saturation that succeeds in reproducing neutron stars phenomenology.

8 Conclusion

In this paper, we have computed neutron star mass-radius curves for stable static stars in the Witten-Sakai-Sugimoto model. Due to the approximation of using the homogeneous Ansatz, we acknowledge that the results are not expected to be trustable at very low densities below saturation density. We have thus constructed a hybrid equation of state by patching the SLy4 EOS and two other EOSs, namely the stiff and soft limit coming from CEFT, together with that of the holographic WSS model, taking into account the symmetry energy, charge neutrality and β -equilibrium. The calibration of the model in this paper, has been chosen by fixing the saturation density to the physical one; this fixed the mass scale M_{KK} of the model and furthermore fixed the symmetry energy to the phenomenologically accepted value at saturation density, by adjusting the 't Hooft coupling. We have calculated everything for two fits, corresponding to the upper (solid lines) and lower (dashed lines) value of the error bar on the symmetry energy. The results we find are unexpectedly good for a top-down holographic QCD model. In particular, we find a large maximal mass between $2.26M_{\odot}$ and $2.35M_{\odot}$, which is hard to achieve for many nuclear physics and phenomenologically driven models. In addition, we pass the current mass-radius constraints as well as the constraints on the tidal deformability (the latter only for one of the fits).

There are many small improvements that could be made, in order to further refine the results and hence to achieve precision neutron star phenomenology from a top-down holographic QCD (WSS) based model. In particular, we have not included the strange quark (s) in the model, but since we also have not included quark masses, those should be incorporated too, in order to achieve a physical model. Furthermore, we have considered the hybrid model of patching together the SLy4 with our holographic WSS results, but the low-density equation of state could in principle be derived from the WSS model by taking into account pasta phases, which in turn would require many more computations such as wall tensions etc. Another refinement of the model would be to take into account higher-order corrections due to the isospin asymmetry, which would correspond to $(\boldsymbol{\chi} \cdot \boldsymbol{\chi})^2$ terms. In principle, the WSS model itself also predicts more accurate higher-order corrections, one example is to consider the full Dirac-Born-Infeld action instead of the leading Yang-Mills term and there are also corrections in $1/N_c$ and $1/\lambda$, although computing those may be unpractical.

On top of these minor refinements, there are also more substantial improvements we can make, that involve changing considerably our construction. These are aimed at removing

qualitative flaws, which we briefly review here, while at the same time providing proposals to remove or at least reduce each of the problems:

- The WSS model only has two free parameters in this configuration: this means that if we fit saturation density and symmetry energy, the chemical potential at the baryon onset is determined. It happens that these choices and the configuration of the homogeneous Ansatz largely overestimate the value of the chemical potential at said onset, introducing the horizontal segment in the EOSs we constructed. We can try to ameliorate this issue by refining the description of nuclear matter as the density decreases towards saturation, for example putting solitonic baryons on a lattice. At the same time, we should change the values of the fit parameters to accommodate for the changes introduced. It is not clear if these two effects will lower the value of the chemical potential, but it seems natural to consider a configuration with resolved individual baryons at such densities: it is after all exactly at the boundary of the region within which we can deem the homogeneous approximation to be reliable.
- The speed of sound exhibits a sharp discontinuity at the junction density: this is not a realistic feature, especially since the transition density is very close to saturation. Around saturation density, the speed of sound is expected to be considerably lower than the values we obtain: following the same reasoning as for the previous point, it is reasonable to attribute this unphysical behavior to the inadequacy of the homogeneous Ansatz at saturation density. The introduction of an intermediate lattice phase could help with this issue, even though it is highly unlikely that we can reach a continuous speed of sound with the hybrid approach.
- The speed of sound keeps growing monotonically until the TOV densities and beyond for a wide range of densities. It is expected that at the TOV scale, matter in neutron stars exhibit deconfinement, hence being in a quark phase. This is a possibility we did not explore in this work, and is certainly an interesting direction for future work: in particular, the TOV masses we find are in the allowed region, but rather large for a static object, and introducing the effects of a high-density quark phase could potentially lower the TOV mass. The introduction of such a phase requires a major change in the setup of the model: in particular, since the introduction of the backreaction from the baryons on the geometry seems an extremely difficult problem to solve, the quark phase can be modeled instead in the non-antipodal setup of the flavor branes, working in the deconfined geometry in the decompactified limit. It is not clear to us at the moment if such a substantial change can be performed while preserving the nice agreement with observations that we have obtained in the present work.

We keep these three points as a guideline for future works.

Acknowledgments

The work of L. B. is supported by the National Natural Science Foundation of China (Grant No. 12150410316). S. B. G. thanks the Outstanding Talent Program of Henan University and the Ministry of Education of Henan Province for partial support. The work of S. B. G. is supported by the National Natural Science Foundation of China (Grants No. 11675223 and No. 12071111) and by the Ministry of Science and Technology of China (Grant No. G2022026021L).

References

- [1] A. Kurkela, P. Romatschke, and A. Vuorinen, *Cold Quark Matter*, *Phys. Rev. D* **81** (2010) 105021, [[arXiv:0912.1856](#)].
- [2] J. M. Maldacena, *The Large N limit of superconformal field theories and supergravity*, *Adv. Theor. Math. Phys.* **2** (1998) 231–252, [[hep-th/9711200](#)].
- [3] E. Witten, *Anti-de Sitter space, thermal phase transition, and confinement in gauge theories*, *Adv. Theor. Math. Phys.* **2** (1998) 505–532, [[hep-th/9803131](#)].
- [4] T. Sakai and S. Sugimoto, *Low energy hadron physics in holographic QCD*, *Prog. Theor. Phys.* **113** (2005) 843–882, [[hep-th/0412141](#)].
- [5] T. Sakai and S. Sugimoto, *More on a holographic dual of QCD*, *Prog. Theor. Phys.* **114** (2005) 1083–1118, [[hep-th/0507073](#)].
- [6] N. Kovensky, A. Poole, and A. Schmitt, *Building a realistic neutron star from holography*, *Phys. Rev. D* **105** (2022), no. 3 034022, [[arXiv:2111.03374](#)].
- [7] T. Demircik, C. Ecker, M. Järvinen, L. Rezzolla, S. Tootle, and K. Topolski, *Exploring the Phase Diagram of V-QCD with Neutron Star Merger Simulations*, *EPJ Web Conf.* **274** (2022) 07006, [[arXiv:2211.10118](#)].
- [8] C. Hoyos, D. Rodríguez Fernández, N. Jokela, and A. Vuorinen, *Holographic quark matter and neutron stars*, *Phys. Rev. Lett.* **117** (2016), no. 3 032501, [[arXiv:1603.02943](#)].
- [9] K. Bitaghsir Fadafan, J. Cruz Rojas, and N. Evans, *Deconfined, Massive Quark Phase at High Density and Compact Stars: A Holographic Study*, *Phys. Rev. D* **101** (2020), no. 12 126005, [[arXiv:1911.12705](#)].
- [10] K. Bitaghsir Fadafan, J. Cruz Rojas, and N. Evans, *Holographic quark matter with colour superconductivity and a stiff equation of state for compact stars*, *Phys. Rev. D* **103** (2021), no. 2 026012, [[arXiv:2009.14079](#)].

- [11] L. Bartolini, S. B. Gudnason, J. Leutgeb, and A. Rebhan, *Neutron stars and phase diagram in a hard-wall AdS/QCD model*, *Phys. Rev. D* **105** (2022), no. 12 126014, [[arXiv:2202.12845](#)].
- [12] M. Järvinen, *Holographic modeling of nuclear matter and neutron stars*, *Eur. Phys. J. C* **82** (2022), no. 4 282, [[arXiv:2110.08281](#)].
- [13] C. Hoyos, N. Jokela, and A. Vuorinen, *Holographic approach to compact stars and their binary mergers*, *Prog. Part. Nucl. Phys.* **126** (2022) 103972, [[arXiv:2112.08422](#)].
- [14] H. Hata, T. Sakai, S. Sugimoto, and S. Yamato, *Baryons from instantons in holographic QCD*, *Prog. Theor. Phys.* **117** (2007) 1157, [[hep-th/0701280](#)].
- [15] S. Bolognesi and P. Sutcliffe, *The Sakai-Sugimoto soliton*, *JHEP* **01** (2014) 078, [[arXiv:1309.1396](#)].
- [16] K. Zhang, T. Hirayama, L.-W. Luo, and F.-L. Lin, *Compact Star of Holographic Nuclear Matter and GW170817*, *Phys. Lett. B* **801** (2020) 135176, [[arXiv:1902.08477](#)].
- [17] N. Kovensky and A. Schmitt, *Isospin asymmetry in holographic baryonic matter*, *SciPost Phys.* **11** (2021), no. 2 029, [[arXiv:2105.03218](#)].
- [18] L. Bartolini and S. B. Gudnason, *Symmetry energy in holographic QCD*, [[arXiv:2209.14309](#)].
- [19] K. Hashimoto, T. Sakai, and S. Sugimoto, *Holographic Baryons: Static Properties and Form Factors from Gauge/String Duality*, *Prog. Theor. Phys.* **120** (2008) 1093–1137, [[arXiv:0806.3122](#)].
- [20] S. Baldino, L. Bartolini, S. Bolognesi, and S. B. Gudnason, *Holographic Nuclear Physics with Massive Quarks*, *Phys. Rev. D* **103** (2021), no. 12 126015, [[arXiv:2102.00680](#)].
- [21] M. Rozali, H.-H. Shieh, M. Van Raamsdonk, and J. Wu, *Cold Nuclear Matter In Holographic QCD*, *JHEP* **01** (2008) 053, [[arXiv:0708.1322](#)].
- [22] M. Elliot-Ripley, P. Sutcliffe, and M. Zamaklar, *Phases of kinky holographic nuclear matter*, *JHEP* **10** (2016) 088, [[arXiv:1607.04832](#)].
- [23] S.-w. Li, A. Schmitt, and Q. Wang, *From holography towards real-world nuclear matter*, *Phys. Rev. D* **92** (2015), no. 2 026006, [[arXiv:1505.04886](#)].
- [24] J. Cruz Rojas, T. Demircik, and M. Järvinen, *Popcorn Transitions and Approach to Conformality in Homogeneous Holographic Nuclear Matter*, *Symmetry* **15** (2023), no. 2 331, [[arXiv:2301.03173](#)].

- [25] L. Bartolini and S. B. Gudnason, *Boundary terms in the Witten-Sakai-Sugimoto model at finite density*, [arXiv:2309.16328](#).
- [26] N. Kovensky, A. Poole, and A. Schmitt, *Predictions for neutron stars from holographic nuclear matter*, *SciPost Phys. Proc.* **6** (2022) 019, [[arXiv:2112.10633](#)].
- [27] O. Komoltsev and A. Kurkela, *How Perturbative QCD Constrains the Equation of State at Neutron-Star Densities*, *Phys. Rev. Lett.* **128** (2022), no. 20 202701, [[arXiv:2111.05350](#)].
- [28] K. Hebeler, J. M. Lattimer, C. J. Pethick, and A. Schwenk, *Equation of state and neutron star properties constrained by nuclear physics and observation*, *Astrophys. J.* **773** (2013) 11, [[arXiv:1303.4662](#)].
- [29] F. Douchin and P. Haensel, *A unified equation of state of dense matter and neutron star structure*, *Astron. Astrophys.* **380** (2001) 151, [[astro-ph/0111092](#)].
- [30] P. Haensel and B. Pichon, *Experimental nuclear masses and the ground state of cold dense matter*, *Astron. Astrophys.* **283** (1994) 313, [[nucl-th/9310003](#)].
- [31] K. Bitaghsir Fadafan, F. Kazemian, and A. Schmitt, *Towards a holographic quark-hadron continuity*, *JHEP* **03** (2019) 183, [[arXiv:1811.08698](#)].
- [32] E. Annala, T. Gorda, J. Hirvonen, O. Komoltsev, A. Kurkela, J. Nättilä, and A. Vuorinen, *Strongly interacting matter exhibits deconfined behavior in massive neutron stars*, [arXiv:2303.11356](#).
- [33] F. Bigazzi and A. L. Cotrone, *Holographic QCD with Dynamical Flavors*, *JHEP* **01** (2015) 104, [[arXiv:1410.2443](#)].
- [34] N. Kovensky and A. Schmitt, *Heavy Holographic QCD*, *JHEP* **02** (2020) 096, [[arXiv:1911.08433](#)].
- [35] N. Kovensky and A. Schmitt, *Holographic quarkyonic matter*, *JHEP* **09** (2020) 112, [[arXiv:2006.13739](#)].
- [36] Y. Lim and J. W. Holt, *Neutron Star Radii, Deformabilities, and Moments of Inertia from Experimental and Ab Initio Theory Constraints of the ^{208}Pb Neutron Skin Thickness*, *Galaxies* **10** (2022), no. 5 99, [[arXiv:2204.09000](#)].
- [37] T. E. Riley et al., *A NICER View of the Massive Pulsar PSR J0740+6620 Informed by Radio Timing and XMM-Newton Spectroscopy*, *Astrophys. J. Lett.* **918** (2021), no. 2 L27, [[arXiv:2105.06980](#)].
- [38] **LIGO Scientific, Virgo** Collaboration, B. P. Abbott et al., *GW170817: Measurements of neutron star radii and equation of state*, *Phys. Rev. Lett.* **121** (2018), no. 16 161101, [[arXiv:1805.11581](#)].